GL04084

ELECTRICAL RESISTIVITY SURVEY McGREGOR RANGE AREA, NEW MEXICO

by

Howard P. Ross, Claron E. Mackelprang, and James C. Witcher

Completed for

Southwest Technology Development Institute
New Mexico State University

Energy & Geoscience Institute
Department of Civil & Environmental Engineering
University of Utah
Salt Lake City, Utah 84108

April 30, 1998

ELECTRICAL RESISTIVITY SURVEY
McGREGOR RANGE AREA, NEW MEXICO

SUMMARY

A dipole-dipole electrical resistivity survey was carried out in the McGregor Range area of the Fort Bliss Military Reservation in November 1997. The survey was completed as one part of an integrated geothermal exploration effort being undertaken by Fort Bliss (Department of the Army) and New Mexico State University.

Seven profiles were completed in an area of approximately 6.5 km^2 (2.5 mi^2) surrounding Davis Dome. The survey maps the electrical resistivity distribution to depths of about 300 m (1000 ft). Very low (1 ohm-m) electrical resistivity zones near Davis Dome indicate a complex upflow area of thermal fluids, and the outflow of these fluids in a subsurface aquifer at shallow depths. The upflow area is associated with faults mapped by Witcher (1997) which bound the Davis Dome topographic feature. Numerical modeling of the resistivity data indicates that low-resistivity layers occur at depths of about 75-100 m (250-350 ft) near Davis Dome and about 150 m (500 ft) at the McGregor Range base facilities. The observed static water levels in all drill holes reported by Witcher (1997) ranged from 137-145 m (450-475 ft) depths. The low-resistivity layers above the static water table may indicate perched water in basin fill above bedrock but in general the low-resistivity bodies correspond to thermal fluids.

INTRODUCTION

An extensive low- to moderate-temperature geothermal resource, now known as the McGregor geothermal system (Witcher, 1997) occurs in the southern Tularosa basin, about 20 to 25 miles (32 to 40 km) northeast of El Paso, Texas (Fig.1). The collocation of this resource with the McGregor Range Base Camp provides an opportunity for utilization of the geothermal fluids.

The U.S. Army Air Defense Artillery Center and Fort Bliss, Directorate of Public Works and Logistics, El Paso, Texas have sponsored a number of geologic studies by the Southwest Technology Development Institute (SWTDI) at New Mexico State University (NMSU) to evaluate the geothermal potential and possible utilization of this geothermal resource. These studies include geologic mapping, a radon soil-gas survey, a soil mercury survey, a detailed self-potential survey, and a shallow temperature-gradient and heat flow survey. Witcher (1997) reviews these studies and their results in some detail. The electrical resistivity survey reported here will aid in the integration of other surface and subsurface data and may aid in siting future production wells. NMSU issued subcontracts to the Energy & Geoscience Institute, University of Utah (EGI/UU) and Consolidated Geophysical Surveys (CGS) for the completion of this resistivity survey and the interpretation of the resulting data.

GEOLOGICAL SETTING

The geology of the survey area has been studied and reported by several authors, and those aspects of the geology most relevant to the geothermal occurrence are summarized by

Witcher, (1997). Witcher notes that the McGregor geothermal system is located along the eastern hinge or flexural margin of a major Rio Grande rift half-graben complex, the Tularosa-Hueco Basin described by Woodward et al. (1978). Seismic and gravity survey interpretations suggest that nearly 2,740 m (9,000 ft) of basin-fill sediments fill the half graben a few miles east of the surface expression of the East Franklin Mountains boundary fault. Bedrock outcrops at Davis Dome are the surface expression of a minor intrabasin horst within the half-graben flexural margin, and this intrabasin horst appears to host the McGregor thermal system (Witcher, 1997). With the exception of Davis Dome, the survey area is a low-relief region covered by thick deposits of sand and silt.

ELECTRICAL RESISTIVITY SURVEY

In the electrical resistivity method, electric current is introduced into the earth at a series of electrode positions and voltages are measured at the surface about these electrodes with specialized potential measuring electrodes. The current is introduced as a square wave of varying polarity (time-domain) or low frequency sine wave (frequency-domain) which permits discrimination from most natural or man-caused current signals. The electrodes may be positioned in any of several established geometric layouts (arrays) depending on the survey aims and circumstances.

The dipole-dipole array has been favored for detailed mining, geothermal and environmental studies (Wright et al., 1985) and was selected for this resistivity survey. In the dipole-dipole array, seven current electrodes are placed in a straight line (in line) and at a uniform interval or spacing (a), and connected with heavy duty single-conductor wire to a current transmitter and motor generator. This permits current switching between six transmitting dipoles, each of length "a". Voltages are measured at the surface in line and on either side of the transmitting electrodes; the greater the distance between transmitting and receiving electrodes, the greater the effect of resistivity distributions at depth. The dipole-dipole array permits the collection of a profile data set which varies with position along the profile and with depth.

In this survey, Consolidated Geophysical Surveys (CGS) used a Melano-Pyxis Model P-15C Engine-Generator set which provided power to a Elliot Model 15A time-domain IP (induced polarization) transmitter. Voltage signals were measured with a Fluke Model 27 digital multimeter. Typical transmitter output was 3-5 amps at 400 volts, and this provided adequate signal strength for the dipole lengths and separations being used. The electrical resistivity survey was conducted by a three-man crew including Claron Mackelprang (CGS), Howard Ross (EGI) and James Witcher (NMSU) from November 10-16, 1997.

The area selected for survey coverage was defined by Witcher (1997) from the higher temperature and higher temperature-gradient results of earlier studies. A survey of six to seven lines of 500 ft (150 m) dipoles provided adequate lateral coverage of the area, and the dipole length of 500 feet provided a good compromise between spatial resolution and depth of study, normally about twice the dipole spacing, a, or 1000 feet in this survey.

Electrical Resistivity Results

The survey was completed without major difficulties, although unseasonable rains and a lack of radio communication posed some problems to the effort. By working long days an average production rate of one survey line per day was achieved. The locations of survey lines MR-1 through MR-6 are shown on Figure 2. Detailed data for all profiles, including transmitting and receiving dipoles, transmitted current, observed voltages and the calculated apparent resistivity, are presented in Appendix I. The results are presented in Figures 3-8 in standard format as "psuedosection" plots with horizontal distance scale of 0.5 inch = 500 ft = a. In the psuedosection plot, the apparent resistivity value is plotted at the intersection of 45 degree lines drawn below the transmitting and receiving dipoles. Measurements were made for electrode separations (n) of n=1-6. The first separation, with current penetration near the surface, is plotted at the top and resistivities for n=6 are plotted at the bottom of the psuedosection, representing increased current penetration to depth.

Beneath each psuedosection plot the interpreted resistivity distribution is plotted to true scale, showing the intrinsic or true resistivity for a given geometric body, as opposed to the observed apparent resistivity. The apparent resistivity data and resulting interpreted resistivity distribution for lines 1 through 6 are shown as Figures 3 through 8.

CGS completed numerical model solutions for Lines 1, 2, 4, and 6. Lines 3 and 5 showed a somewhat simpler resistivity distribution, and an interpreted true scale resistivity distribution for these lines is estimated from the results for Lines 1, 2, and 4 and other model results. The numerical model solutions are our best estimate of the true geometries and intrinsic resistivities. CGS completed the numerical modeling using a PC version of Program IP2D which assumes a two-dimensional resistivity distribution (geometry) perpendicular to the orientation of the resistivity line. This condition was not strictly met for all profiles of this survey, but the model results still provide our best estimates of the true resistivities and to-scale geometric relationships. Initial resistivity geometries and values were estimated and the corresponding apparent resistivities were computed for comparison with the observed data. Model geometries and resistivity values were then modified up to 12 times until a satisfactory "best fit" to the observed data was obtained. These final geometric models must later be interpreted in view of their mapped position, known geologic information, and other geophysical data. Geothermal areas are often typified by low electrical resistivities which arise from the conductive thermal fluids themselves, and accompanying clay alteration minerals which result from the thermal fluids.

Line 1 (Extended). This line was located along a east-northeast-trending dirt road which aligns with the south side of Davis Dome. Station 0 (initial center of the current electrode spread) was located about 200 ft north of well 46-6 which recorded temperatures of 178°F at about 720 ft and 193°F at total depth (about 2140 ft) (R. Jacobson, Sandia National Labs., 1997). Low apparent resistivities of 3-4 ohm-m were observed west of station 6E beneath a moderate resistivity surface layer (Fig.3), and 1-2 ohm-m values were noted at the eastern end of the initial line, on the south side of Davis Dome. Because of these low resistivities, and their possible correlation with large cavities with thermal fluids observed in drilling, Line 1 was extended to the east by establishing current electrodes at stations 6-11. Locally higher resistivities were observed which correspond

to the bedrock horst, adjacent to resistivities <3 ohm-m.

The numerical model was centered at station 6E to provide the most detail for the complex area of high and adjacent low resistivities near Davis Dome. The model shows the high resistivity bodies associated with the bedrock horst, bounded by probable faults, and 1 ohm-m bodies which appear to go to depth. The 1 ohm-m bodies could represent fluids and alteration associated with a major thermal fluid upflow zone along the margins of the horst. A tabular body of 1 and 5 ohm-m resistivities extending west of station 6E appears to be an outflow zone or thermal aquifer, perhaps showing some mixing with cooler ground waters. The western part of the model is inferred from the well-constrained model to the east and from a similar resistivitity disribution for the western half of Line 2 to the north. The computed resistivity values are a good match to the observed data except for n=1 values in the center of the line. Three-dimensional effects probably preclude a better match to a two-dimensional model.

Line 2 was centered at the eastern side of the airfield runway, northeast of Davis Dome. The data (Fig.4) include higher resistivity values (12-63 ohm-m) on the first separation, n=1, corresponding to shallow bedrock, with low resistivities at depth and to the east. The numerical model confirms 100-150 ohm-m resistivities of the limestone horst block extending to depth, background resistivities of 10-20 ohm-m corresponding to a relatively shallow water table in the sandy basin fill, and areas of 1-2 ohm m which probably correspond to saline thermal fluids, and perhaps wall rock alteration. The computed resistivity values are an excellent match to the observed data.

Line 3, a east-trending line south of Davis Dome, is dominated by 5-10 ohm-m apparent resistivities (Fig.5) corresponding mainly to basin-fill deposits. A higher-resistivity diagonal from 3-2 West probably reflects shallow bedrock of 50-100 ohm-m as noted on Lines 1 and 2, and pictured on our estimated resistivity model. Observed apparent resistivities of 2-4 ohm-m arise from a narrow conductive body, possibly a fluid upflow zone, between 0-1W.

Line 4, Figure 6, records some higher resistivities in the near surface beneath the center of the line, and at depth on the eastern end. Low resistivities of 2.5-5 ohm-m occur on n=3,4,5 on the west and rise to the east on n=1,2,3, giving the appearance of a conductive body dipping to the west. The numerical model, which achieved an excellent fit to the observed data, does show a tabular body dipping to the west. The model is quite sensitive to small resistivity changes at depths of 500-1000 feet.

Line 5, Figure 7, shows an apparent resistivity distribution very similar to that of Line 4, with a more continuous near-surface resistive layer, a thicker low resistivity intermediate layer, and then increasing resistivities for the deepest two separations, n=5,6. The estimated resistivity model, based on the successful solution for Line 4 only 500 to 1500 feet to the north, is thought to be a good representation of the true resistivity distribution.

Line 6. This line was completed in a north-south orientation through the McGregor Rang base camp area to provide control on the resistivity distribution near potential user facilities. Intermediate resistivities are noted on n=1,2 (Fig.7) with no real indication of the bedrock horst, or any well-defined fluid upflow zones. Low resistivities of 2.7-5 ohm-m are observed in a

layered manner on n=4,5. The numerical model solution achieved a near-perfect fit to the observed data. It shows a tabular low-resistivity body of about 1 ohm-m about 500 feet deep, extending from station 2 south to station 4 north. We interpret this as the conductive thermal aquifer.

INTERPRETATION

Most interpretation of dipole-dipole data is based on the study of the data in psuedosection form. Numerical modeling of the data, described in the previous section, is the main quantitative technique for resolving the apparent resistivity values into true (intrinsic) resistivities and true depth and geometric relationships. Numerical models for Lines 1 through 6 were presented in Figures 3-8. It is also important to consider the horizontal resistivity distribution.

Horizontal Resistivity Distribution

One simple, relatively unbiased way to evaluate the horizontal resistivity distribution is to contour the observed apparent resistivity values for selected separations, plotting the apparent resistivity value midway between the transmitting and receiving dipoles. Figure 9 shows the contoured apparent resistivity values for the second separation, n=2. The apparent resistivity values for this separation are essentially averaged resistivities for the surface to depths of about 250 feet. Inspection of Figure 9 indicates generally low (1-10 ohm-m) resistivity values for the near surface throughout much of the survey area, with a complex pattern of higher values on the south end of Line 6 and a complex resistivity high (15-41 ohm-m) near Davis Dome. Unusually low values (<5 ohm-m) are indicated west, east, and south of Davis Dome.

Figure 10 shows contoured apparent resistivities for n=4, corresponding to depths of about 400-700 feet with some surface effects included. It shows north to north-west contours separating high and lower resistivity values at depth in the Davis Dome area. This suggests a faulting pattern of similar trend within the bedrock. The contour trends are similar to those of the self-potential (SP) map reported by Ross and Witcher (1995) in this area. The resistivity low at Station 0 on Line 1 correlates directly with anomaly SP-2 of that survey. Figure 11summarizes SP anomalies and temperature gradient anomalies (Witcher, 1997) for comparison with the resistivity data.

A more useful way to evaluate the horizontal resistivity distribution is to plot the resistivity bodies and intrinsic resistivities determined from modeling and interpretation, for specific depth intervals or slices. Figure 12 shows the resistivity distribution for the depth interval 250-350 feet. Very low-resistivity bodies of 1 and 2 ohm-m occur near Davis Dome and over a broad area to the south on Lines 4 and 5. The low values near Davis Dome occur near or within the 350°C/km temperature gradient contour of Figure 11.

Figure 13 presents the resistivity slice for depths of 500-750 feet. Low-resistivity zones near Davis Dome are still present but the broad area to the south is now background 10 ohm-m values, suggesting the upper low-resistivity zone may be a plume or perched water in basin fill

deposits. A 1 ohm-m zone is indicated on Line 6, within the Base Camp, that is probably due to thermal fluids, possibly near an upflow zone. Several possible fault locations have been inferred and are plotted on this map. Faults east of the south-trending blacktop road to Meyer Range offset surficial deposits with down-to-east hanging walls (Witcher, 1997).

Figure 14 shows the interpreted resistivity values for the depth interval 750-1000 feet. This is the deepest resistivity "slice" we believe can be justified by the data and modeling, and the resolution of body borders is less accurate. We note low-resistivity zones of 1 and 3 ohm-m near Davis Dome which may relate to thermal fluid conduits from depth. The 1 ohm-m zone beneath the Base Camp area is also present at this depth.

DISCUSSION

Figures 12, 13, and 14 are easily correlated with the temperature gradient and SP anomalies of Figure 11 by overlaying the maps. We find some correlation with both temperature and SP anomalies for all depths and lines, except Line 6 where no SP data are available. Table I below summarizes these correlations.

Table 1. Spatial Correlation Matrix, Resistivity, Temperature Gradient and SP Data

Resistivity	Temperature Gradients			Resistivity	SP Anomalies		
Line 2	S	I	D	Line 2	S: 1 east;	I: 1 east;	----
Line 1	S	I	D	Line 1	S: 1 south;	I: 2;	D: 1south
Line 3	---	I	D	Line 3	----------	---------	-----
Line 4	S	---	---	Line 4	S: 1 south;	---------	-----
Line 5	S	---	---	Line 5	S: 3 north;	---------	-----
Line 6	---	I	D	Line 6	NA	NA	NA

where the correlation is with low resistivity (1-3 ohm-m) zones for the depth slices identified as: S=shallow (250-350 ft); I=intermediate (500-750 ft); and D=deep (750-1000 ft).

Intermediate- to high-temperature geothermal areas throughout the world are characterized by low electrical resistivities. The low resistivities are due to the conductive thermal fluids themselves, and the associated alteration minerals, especially clay and mica minerals. Observed (apparent) resistivities of 3-5 ohm-m are common (Wright et al., 1985) while observed and modeled resistivities of less than 3 ohm-m are less common, for bulk volumes. Electrical resistivities of 10-30 ohm-m are fairly common for alluvial materials, with lower values often indicating some lake beds and clay layers. In evaluating the results of this study, it appears that upwelling thermal fluids, and relatively undiluted outflow (plume) fluids may be represented by 1-3 ohm-m resistivities. Resistivities of 3-6 ohm-m may indicate some dilution with other ground waters.

Upwelling thermal fluids may be indicated by the low-resistivity bodies which extend to depth on Lines 1, 2 and 3. There is some possibility of a separate upflow zone associated with the deep 1 ohm-m body of Line 6 beneath the Base Camp. Other low-resistivity zones that are

limited to shallow depth probably represent outflow plumes. Several well-defined resistivity contrasts near Davis Dome that are continuous between several profiles are interpreted as faults. Some of these features correspond to faults with possible Pleistocene offset as noted by Witcher (1997).

REFERENCES

Ross, H.P., Blackett, R.E., Shubat, M.A., and Mackelprang, C.E., 1990, Delineation of fluid upflow and outflow plume with electrical resistivity and self-potential data- Newcastle geothermal area, Utah: Geothermal Resources Council Transactions, v.14, Part II, p.1531-1536.

Ross, H.P., and Witcher, J.C., 1992, Self-potential expression of hydrothermal resources in the Southern Rio Grande Rift, New Mexico: Geothermal Resources Council Transactions, v.16, p.247-253.

Ross, H.P., and Witcher, J.C., 1995, Self-potential survey, McGregor Range Fort Bliss Military Reservation, New Mexico: Earth Sciences and Resources Institute, University of Utah, Salt Lake City, ESRI/UU final report to SWTDI/NMSU, 6 p.

Seager, W.R., 1980, Quaternary fault system in the Tularosa and Hueco basins, southern New Mexico and West Texas, in Dickerson, P.W., and Hoffer, J.W., eds., Trans-Pecos Region: New Mexico Geological Society 31st Annual Field Conference Guidebook, p.131-136.

Witcher, J.C., 1997, Geothermal resource potential of McGregor Range, New Mexico: Southwest Technology Development Institute, New Mexico State University, Las Cruces, SWTDI report Geo-97-5, to Mariah Associates, Inc., 26 p.

Woodward, L.A. Callender, J.F., Seager, W.R., Chapin, C.E., Gries, J.C., Shaffer, W.L., and Zilinski, R.E., 1978, tectonic map of Rio Grande rift region in New Mexico, Chihuahua, and Texas, in Hawley, J.W., compiler, Guidebook to Rio Grande Rift in New Mexico and Colorado: New Mexico Bureau of Mines and Mineral Resources Circular 163, map 1:1,000,000 scale.

Wright, P.M., Ward, S.H., Ross, H.P., and West, R.C., 1985, State-of-the Art— Geophysical exploration for geothermal resources: Geophysics, v.50, p.2666-2696.

ILLUSTRATIONS

Figure 1. Location map for the McGregor Range Camp area showing regional geologic features (after Seager, 1980).

Figure 2. Dipole-dipole survey line location map, Lines MR - 1 - MR - 6.

Figure 3. Observed apparent resistivity data and numerical model solution, Line MR-1 & 1 ext.

Figure 4. Observed apparent resistivity data and numerical model solution, Line MR-2.

Figure 5. Observed apparent resistivity data and estimated resistivity model, Line MR-3.

Figure 6. Observed apparent resistivity data and numerical model solution, Line MR-4.

Figure 7. Observed apparent resistivity data and estimated resistivity model, Line MR-5.

Figure 8. Observed apparent resistivity data and numerical model solution, Line MR-6.

Figure 9. Contoured observed apparent resistivity data (ohm-m) for second separation (n=2). Scale 1"=2000 ft.

Figure 10. Contoured observed apparent resistivity data (ohm-m) for fourth separation (n=4). Scale 1"=2000 ft.

Figure 11. Temperature gradient contours (degrees C/km) and SP anomalies in the McGregor Range resistivity survey area. Scale 1"=2000 ft.

Figure 12. Modeled electrical resistivity distribution for the depth interval 250-350 ft. Scale 1"=2000 ft.

Figure 13. Modeled electrical resistivity distribution for the depth interval 500-750 ft. Scale 1"=2000 ft.

Figure 14. Modeled electrical resistivity distribution for the depth interval 750-1000 ft. Scale 1"=2000 ft.

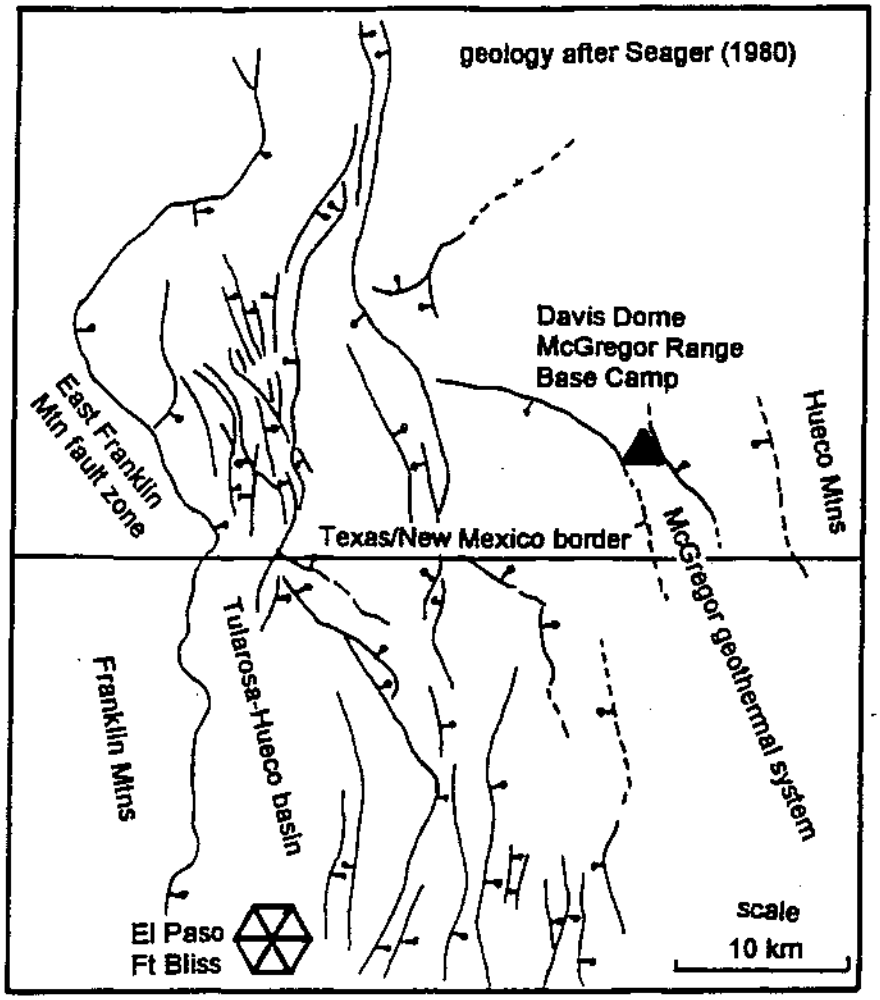

Figure 1. Location map for the McGregor Range Camp area showing regional geologic features (after Seager, 1980).

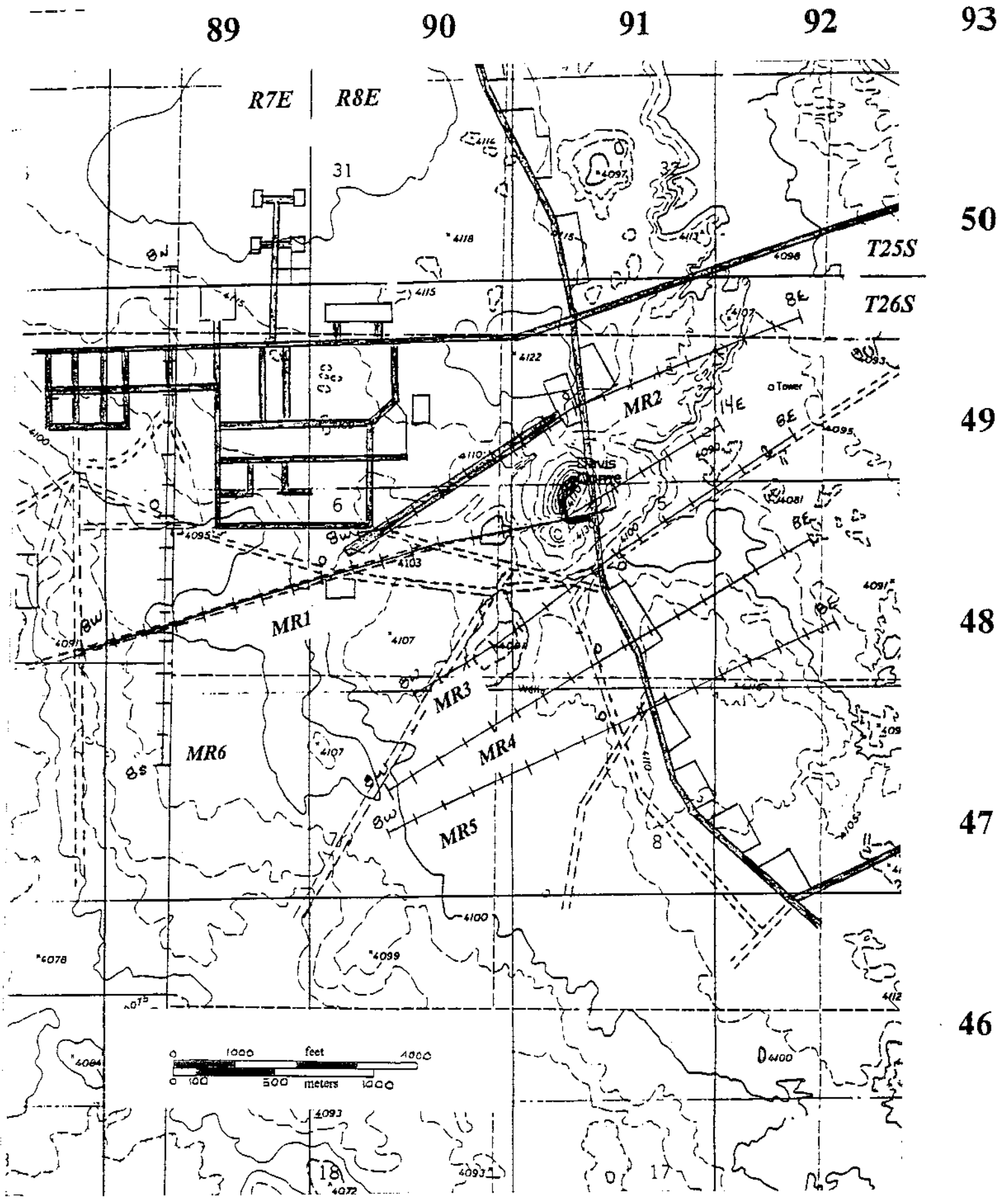

Figure 2. Dipole-dipole survey line location map, Lines MR - 1 - MR - 6.

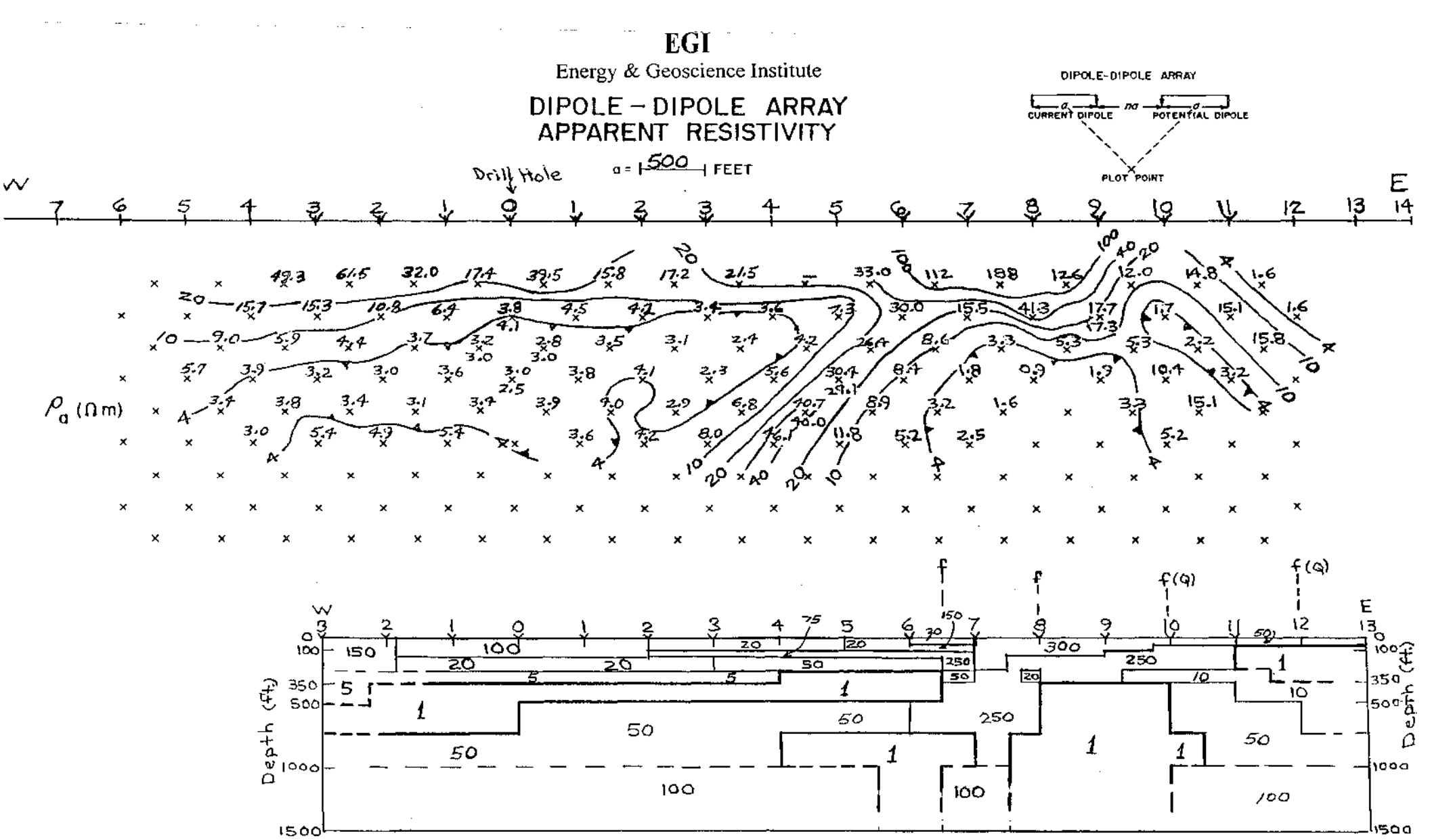

f Possible fault from resistivity

Q Faulted Quaternary Deposits (scarp)

Figure 3. Observed apparent resistivity data and numerical model solution, Line MR-1 & 1 ext.

AREA McGregor Range STATE N. Mexico LINE 1+1 Ext DATA BY CGS DATE 11/15/97 TRANSMITTER Elliot 15A RECEIVER Fluke 27

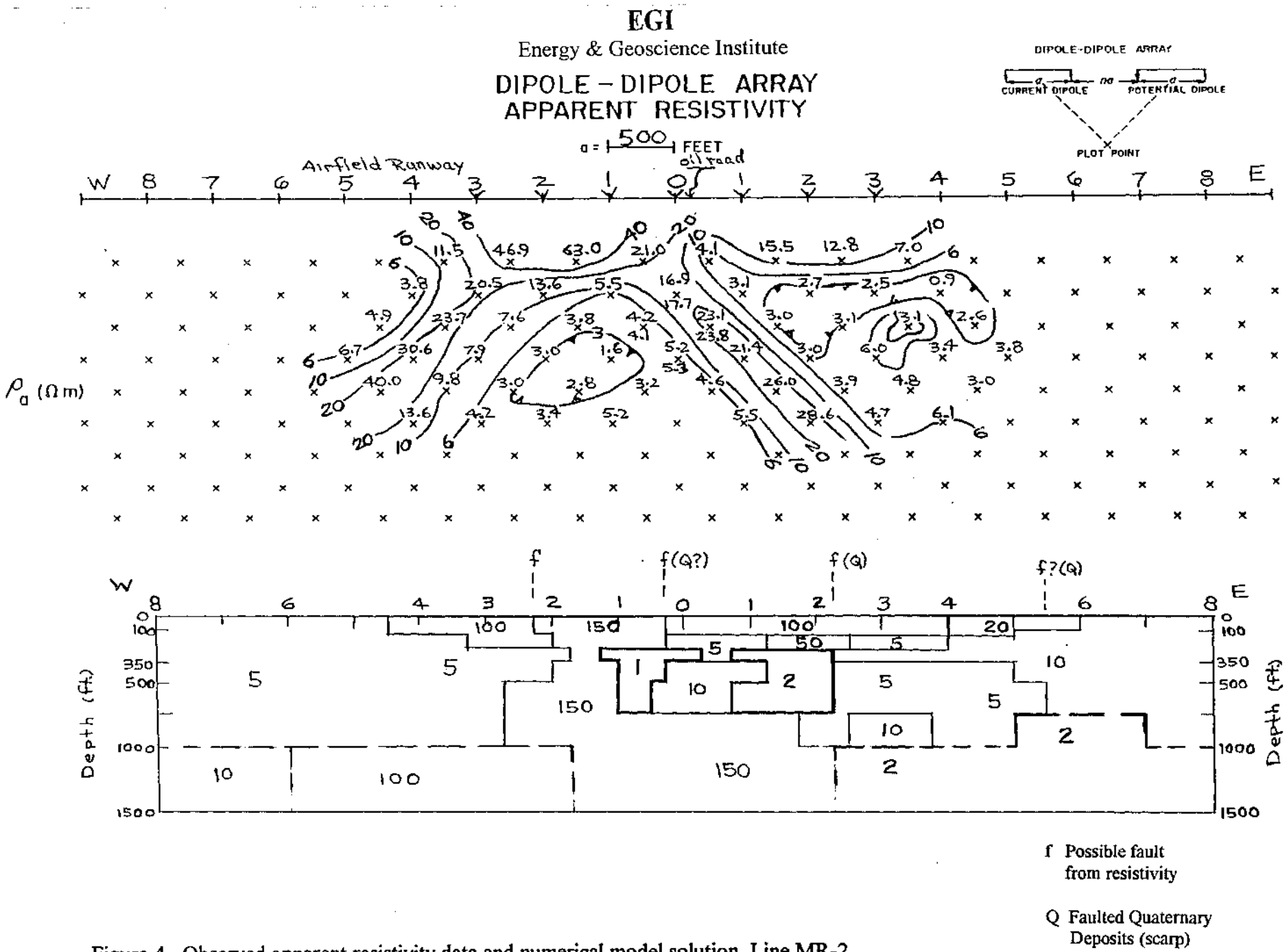

Figure 4. Observed apparent resistivity data and numerical model solution, Line MR-2.

AREA McGregor Range STATE NM LINE 2 DATA BY CGS DATE 11/12/97 TRANSMITTER Elliot ISA RECEIVER Fluke 27

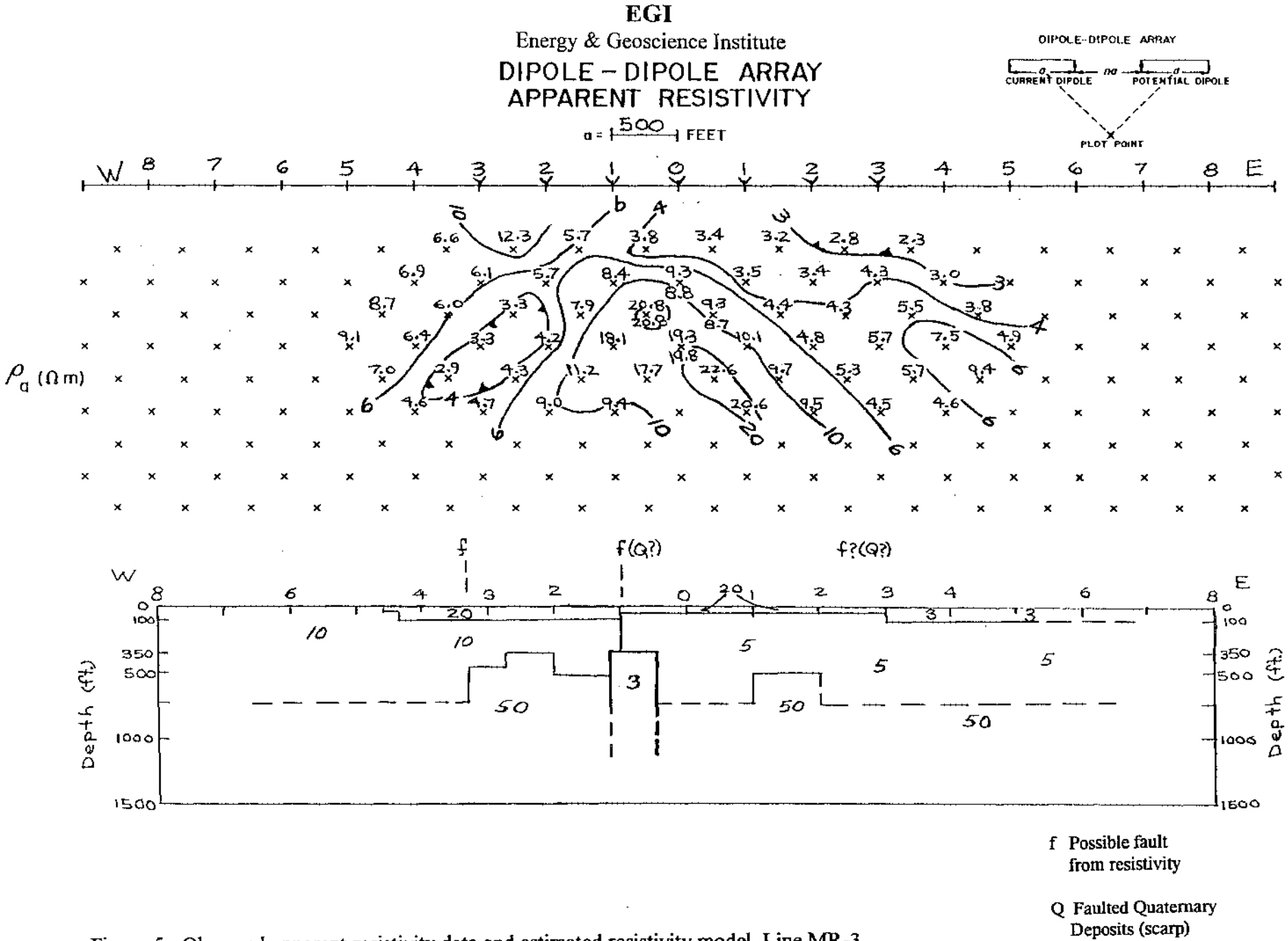

Figure 5. Observed apparent resistivity data and estimated resistivity model, Line MR-3.

AREA McGregor Range STATE NM LINE 3 DATA BY CGS DATE 11/13/97 TRANSMITTER Elliot SA RECEIVER Fluke 27

EGI

Energy & Geoscience Institute

DIPOLE – DIPOLE ARRAY APPARENT RESISTIVITY

a = 500 FEET

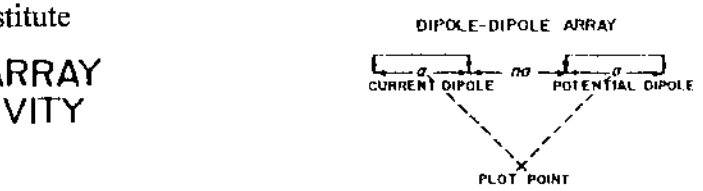

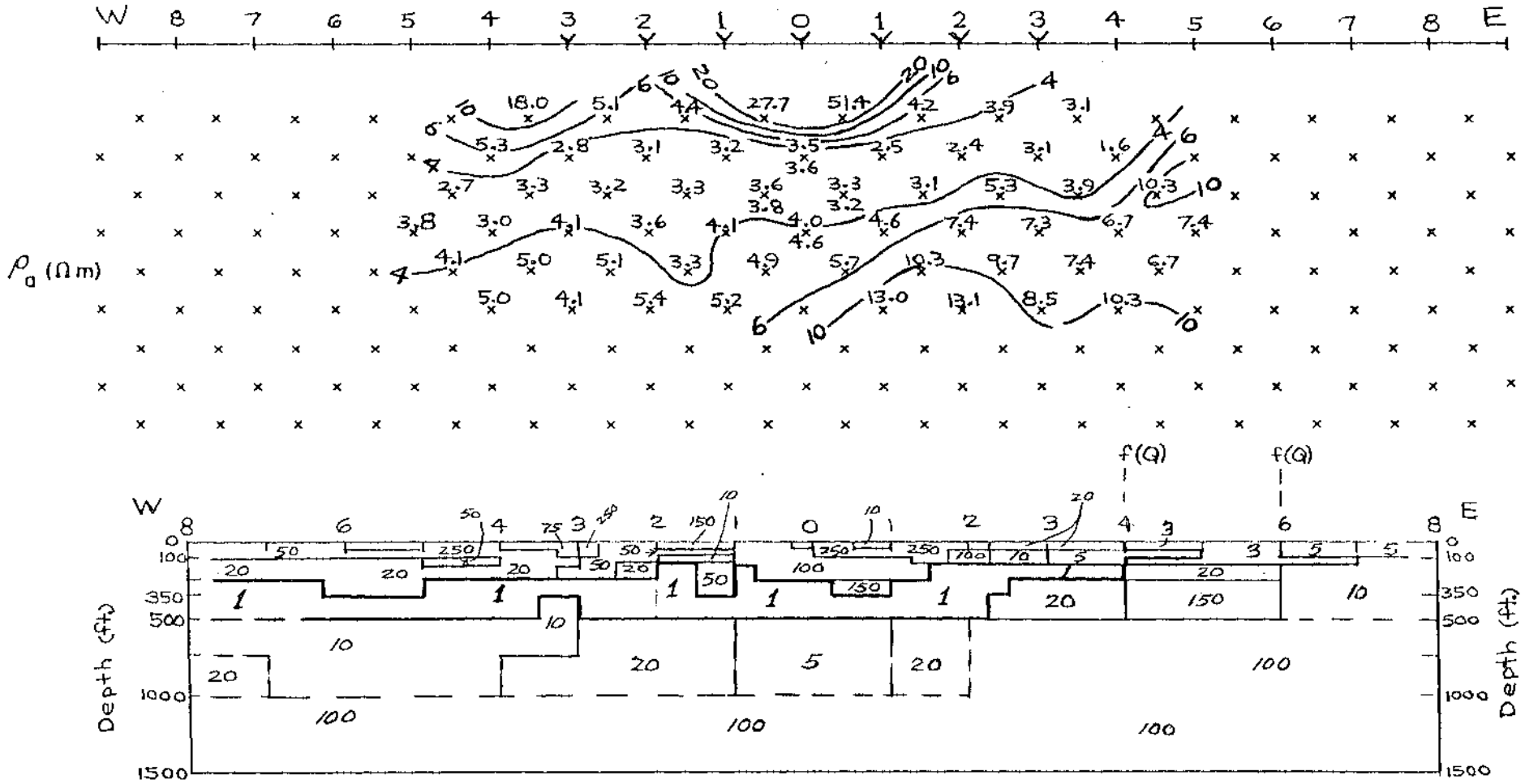

f Possible fault from resistivity

Q Faulted Quaternary Deposits (scarp)

Figure 6. Observed apparent resistivity data and numerical model solution, Line MR-4.

AREA McGregor Range STATE NM LINE 4 DATA BY CGS DATE 11/14/97 TRANSMITTER Elliot 15A RECEIVER Fluke 27

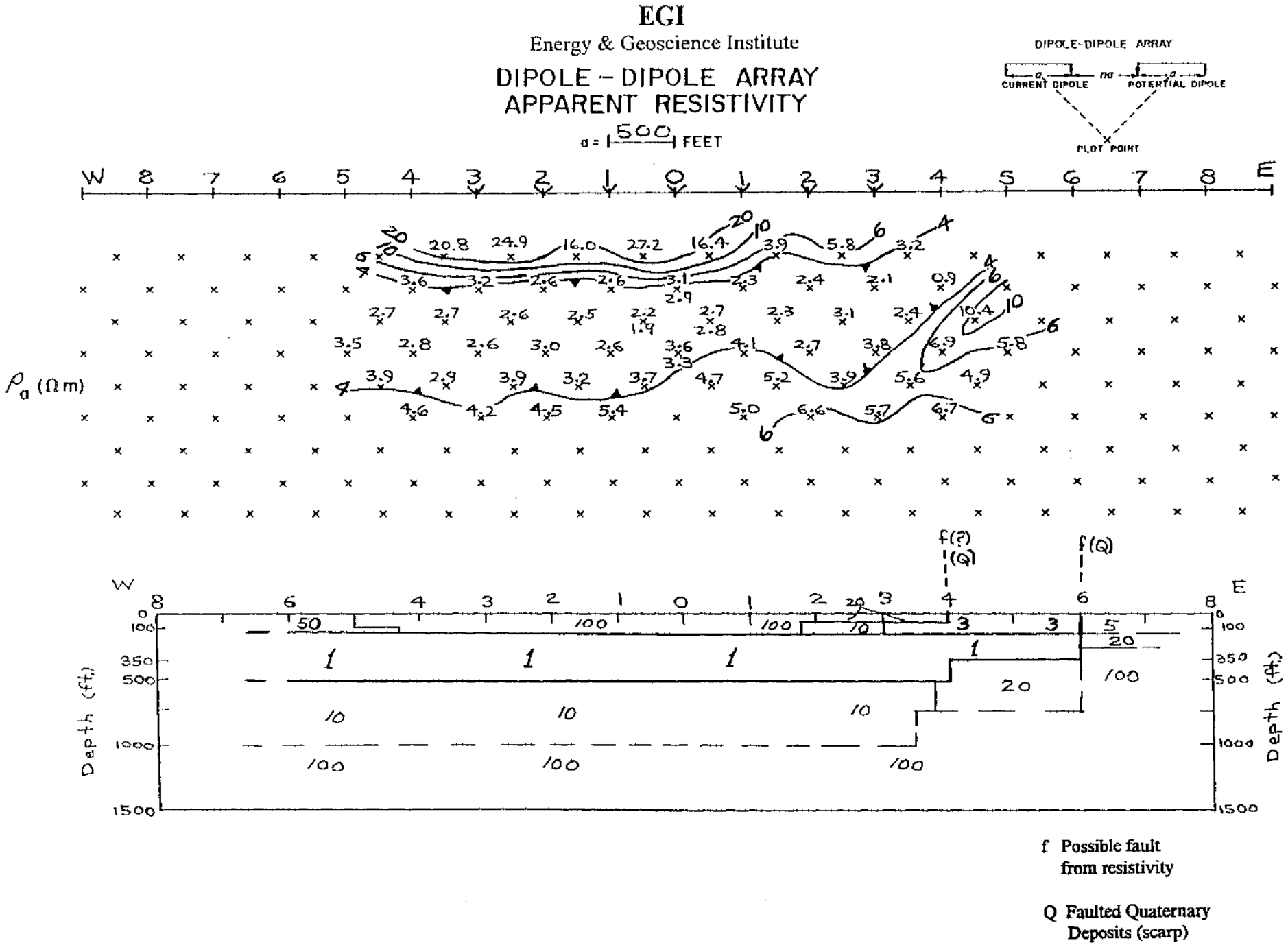

Figure 7. Observed apparent resistivity data and estimated resistivity model, Line MR-5.

AREA McGregor Range STATE NM LINE 5 DATA BY CGS DATE 11/15/97 TRANSMITTER Elliot 15A RECEIVER Fluke 27

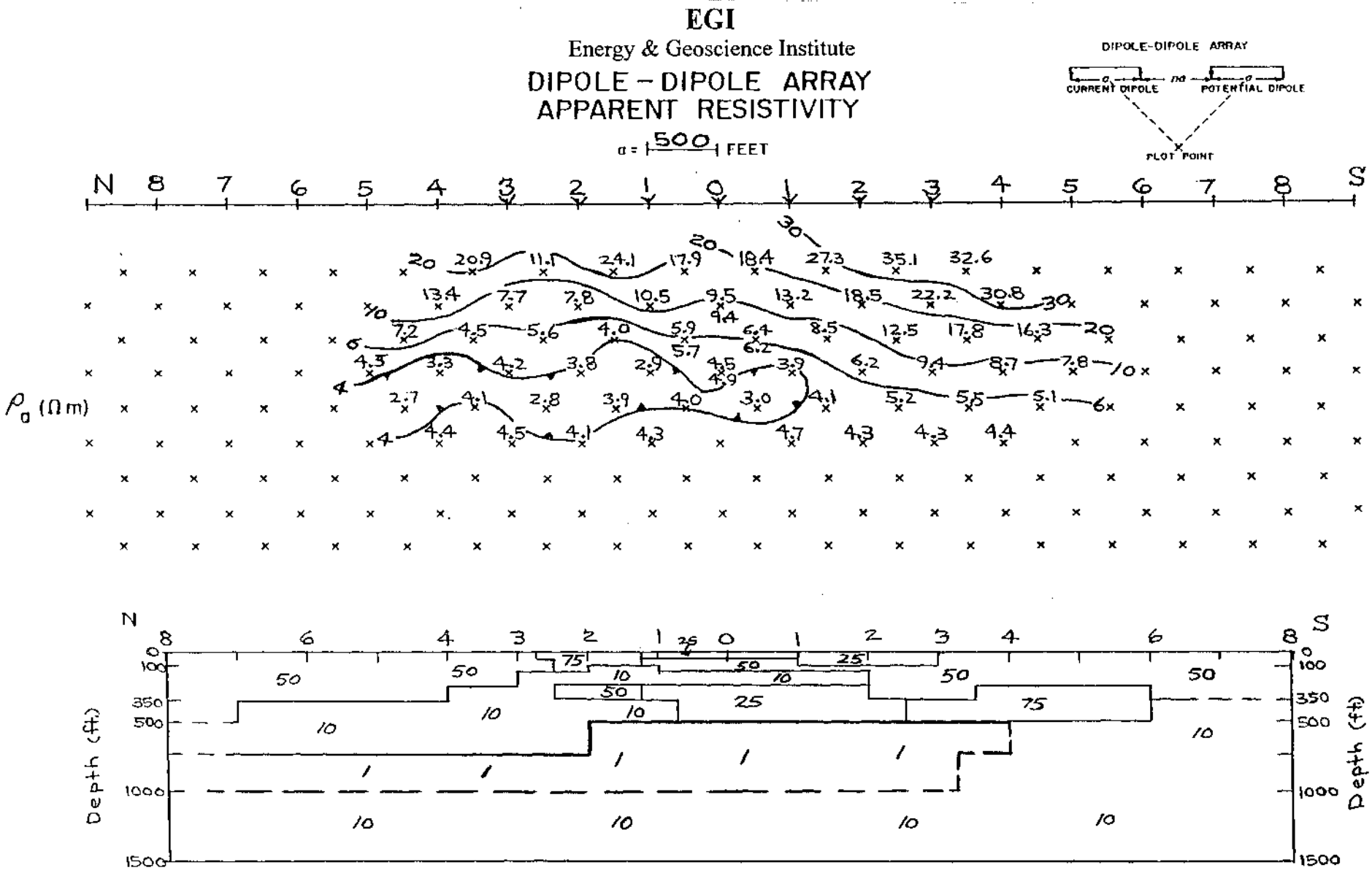

Figure 8. Observed apparent resistivity data and numerical model solution, Line MR-6.

AREA McGregor Range STATE NM LINE 6 DATA BY CGS DATE 11/16/97 TRANSMITTER Elliot 15A RECEIVER Fluke 27

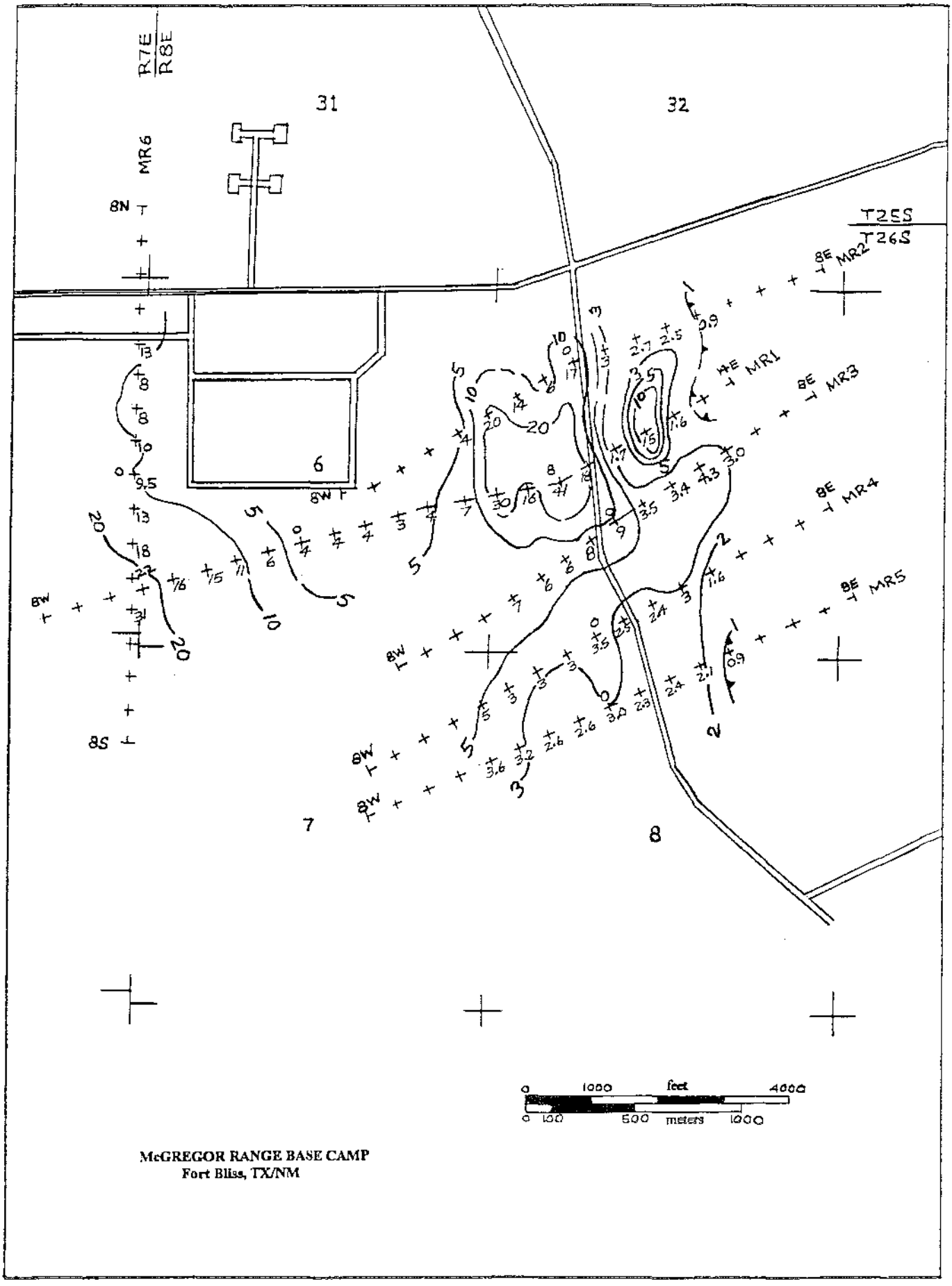

Figure 9. Contoured observed apparent resistivity data (ohm-m) for second separation (n=2). Scale 1"=2000 ft.

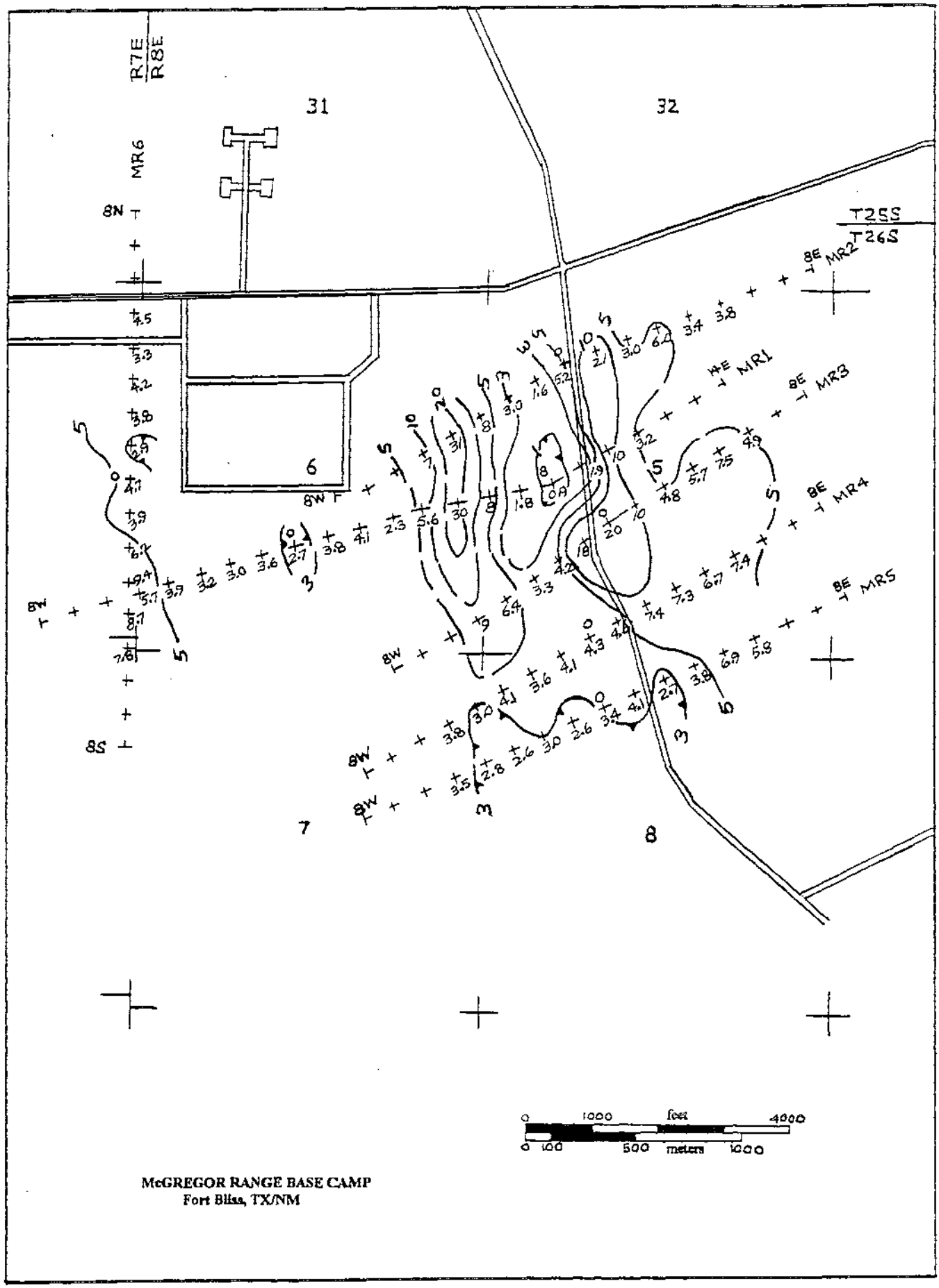

Figure 10. Contoured observed apparent resistivity data (ohm-m) for fourth separation (n=4). Scale 1"=2000 ft.

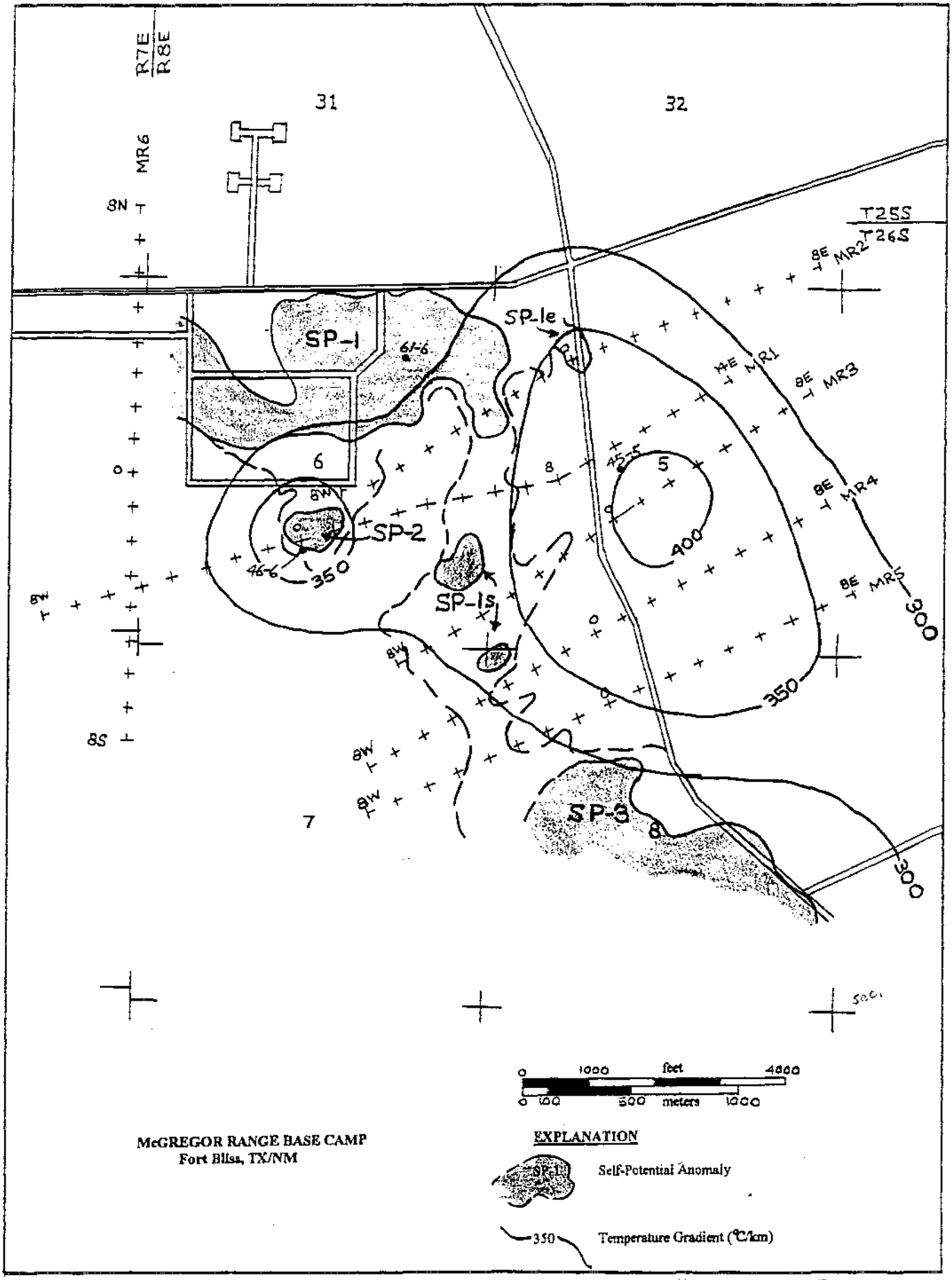

Figure 11. Temperature gradient contours (degrees C/km) and SP anomalies in the McGregor Range resistivity survey area. Scale 1"=2000 ft.

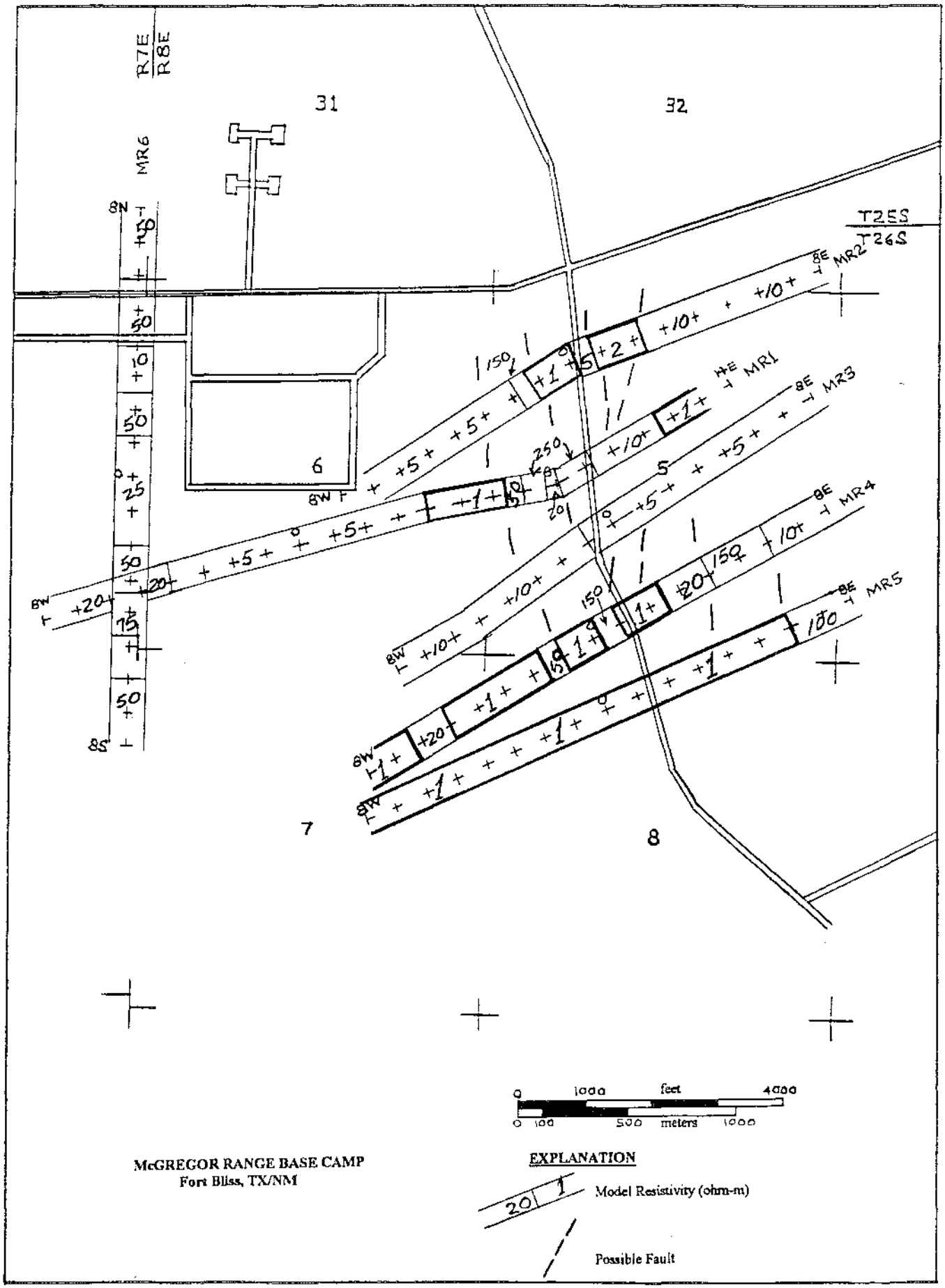

Figure 12. Modeled electrical resistivity distribution for the depth interval 250-350 ft. Scale 1"=2000 ft.

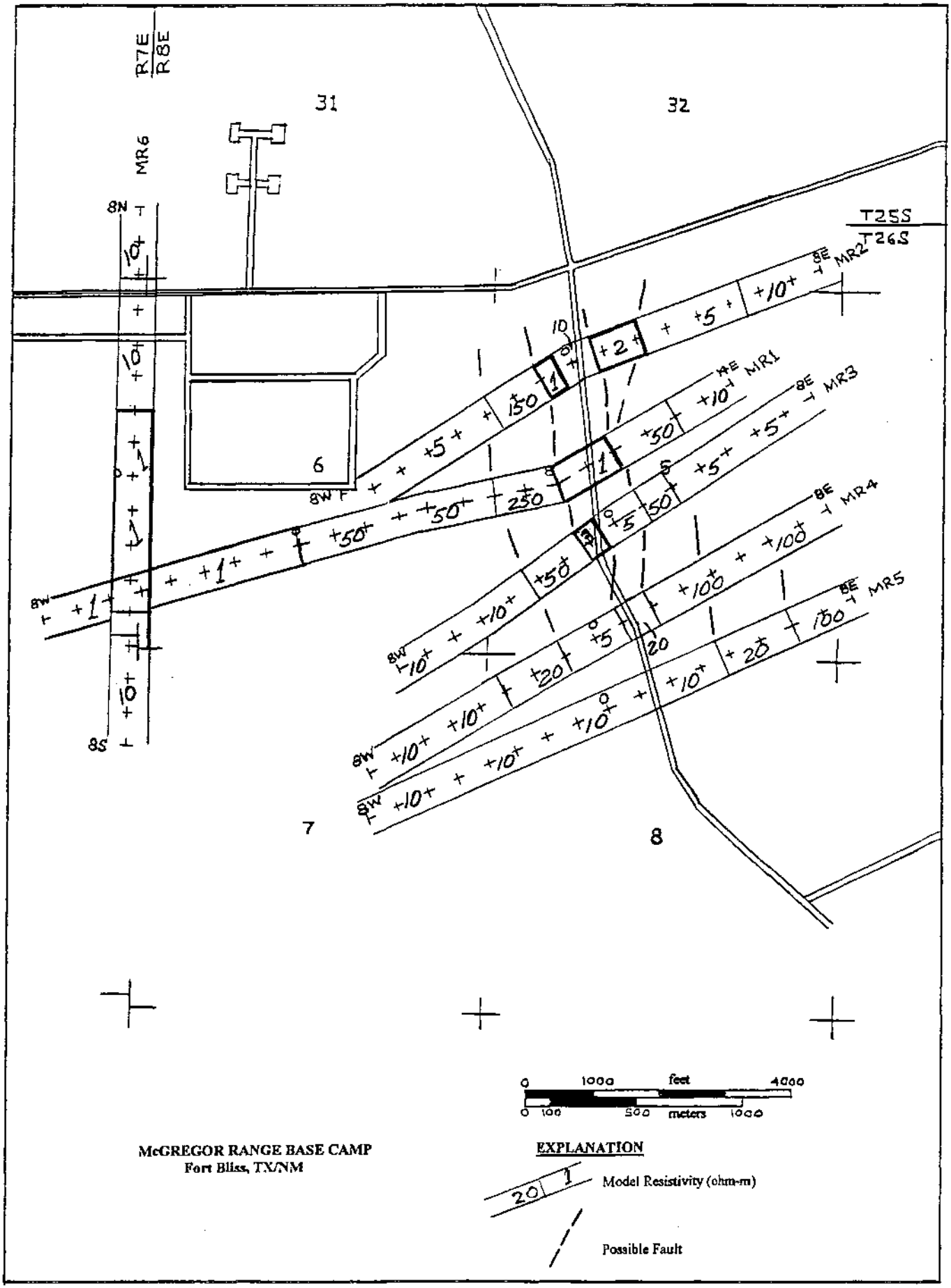

Figure 13. Modeled electrical resistivity distribution for the depth interval 500-750 ft. Scale 1"=2000 ft.

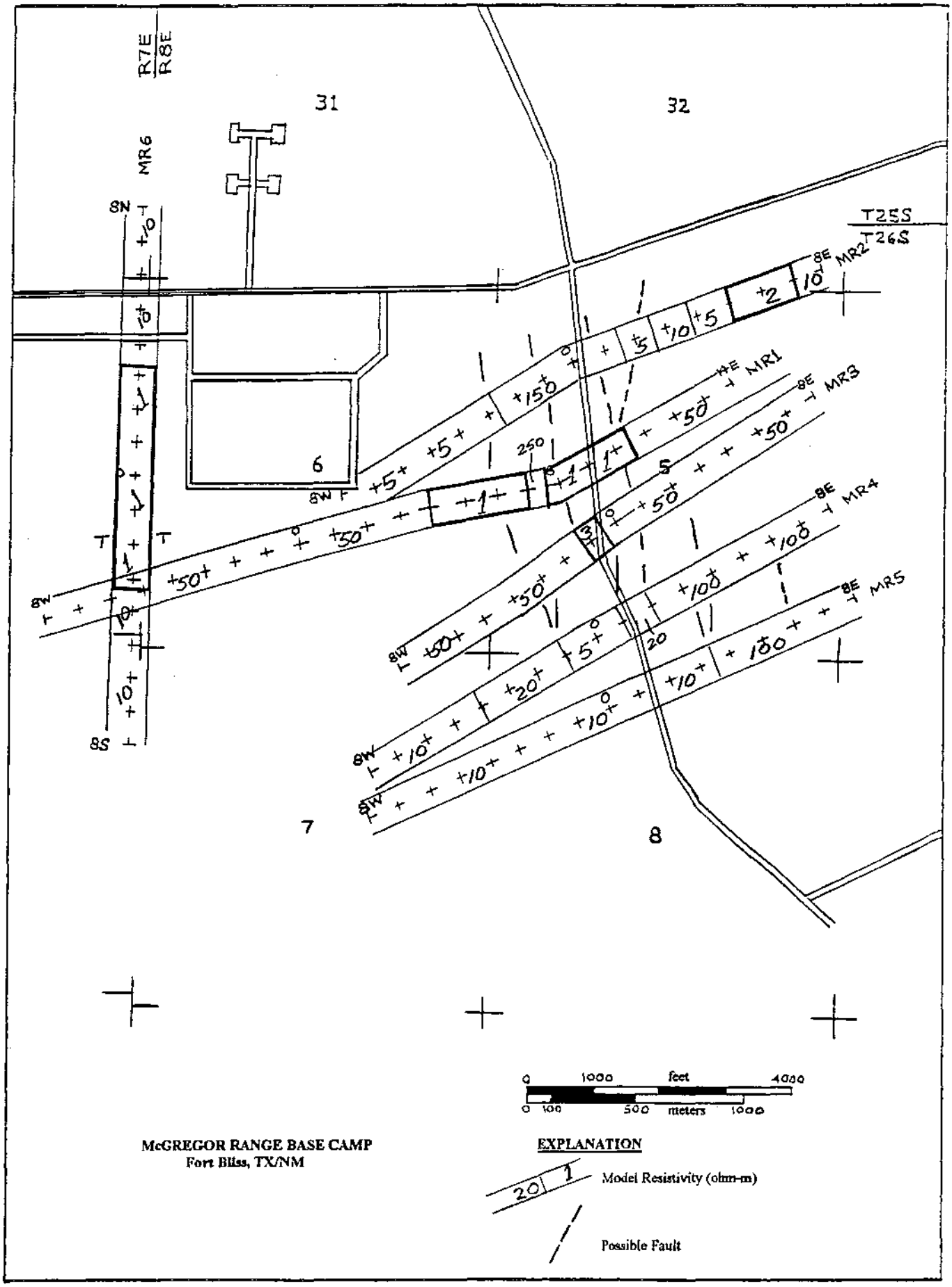

Figure 14. Modeled electrical resistivity distribution for the depth interval 750-1000 ft. Scale 1"=2000 ft.

APPENDIX I

MCGREGOR RANGE RESISTIVITY SURVEY - FIELD DATA LISTING

Dipole-Dipole Electrical Resistivity Survey - Dipole Spacing, a = 500 ft.

TX = Transmitting Dipole; RC = Receiving Dipole; N = Dipole Separation;
I = Transmitted Current, amps; V = Observed Voltage, millivolts (mV);
Pa = Computed Apparent Resistivity (ohm-m)

McGREGOR RANGE PROJECT, NEW MEXICO RESISTIVITY SURVEY 1997						
FIELD DATA		a=500FEET				
TX	RC	N	I(AMPS)	V(mV)	Pa (Ohm.m)	
0-1E	1-2W	1	2.95	35.75	17.4	LINE 1
1-2E	"	2	3.285	2.15	3.8	
2-3E	"	3	3.05	0.6	2.8	
0-1W	2-3W	1	2.66	59.1	31.9	
0-1E	"	2	2.95	3.3	6.4	
1-2E	"	3	3.175	0.7	3.2	
2-3E	"	4	3.05	0.35	3.3	
1-2W	3-4W	1	2.925	125.15	61.5	
0-1W	"	2	2.68	5.05	10.8	
0-1E	"	3	2.9	0.75	3.7	
1-2E	"	4	3.175	0.4	3.6	
2-3E	"	5	2.965	0.2	3.4	
2-3W	4-5W	1	3.74	128.4	49.3	
1-2W	"	2	2.9	7.7	15.3	
0-1W	"	3	2.625	0.8	4.4	
0-1E	"	4	2.92	0.3	3	
1-2E	"	5	3.235	0.2	3.1	
2-3E	"	6	2.965	0.2	5.4	
2-3W	5-6W	2	3.74	10.25	15.7	
1-2W	"	3	2.92	1.2	5.9	
0-1W	"	4	2.69	0.3	3.2	
0-1E	"	5	2.94	0.2	3.4	
1-2E	"	6	3.265	0.2	4.9	
2-3W	6-7W	3	3.75	2.35	9	
1-2W	"	4	2.91	0.4	3.9	
0-1W	"	5	2.68	0.2	3.8	
0-1E	"	6	2.985	0.2	5.4	
2-3W	7-8W	4	3.78	0.75	5.7	
1-2W	"	5	2.96	0.2	3.4	
0-1W	"	6	2.715	0.1	3	
0-1W	1-2E	1	3.6	99.1	39.5	
1-2W	"	2	3.905	2.8	4.1	
2-3W	"	3	4.595	0.95	3	
0-1E	2-3E	1	3.835	42.25	15.8	
0-1W		2	3.575	2.8	4.5	
1-2W	"	3	3.88	0.8	3	
2-3W	"	4	4.51	0.4	2.5	

1-2E	3-4E	1	3.88	46.45	17.2
0-1E	"	2	3.795	2.77	4.2
0-1W	"	3	3.535	0.85	3.5
1-2W	"	4	3.82	0.5	3.8
2-3W		5	4.48	0.35	3.9
2-3E	4-5E	1	3.79	56.65	21.5
1-2E	"	2	3.88	2.3	3.4
0-1E	"	3	3.76	0.8	3.1
0-1W	"	4	3.52	0.5	4.1
1-2W	"	5	3.795	0.3	4
2-3W	"	6	4.475	0.2	3.6
2-3E	5-6E	2	3.785	2.4	3.6
1-2E	"	3	3.815	0.65	2.4
0-1E	"	4	3.76	0.3	2.3
0-1W	"	5	3.51	0.2	2.9
1-2W	"	6	3.8	0.2	4.2
2-3E	6-7E	3	3.78	1.1	4.2
1-2E	"	4	3.815	0.75	5.6
0-1E	"	5	3.72	0.5	6.8
0-1W	"	6	3.5	0.35	8
2-3E	7-8E	4	3.775	4	30.4
1-2E	"	5	3.83	3.1	40.7
0-1E	"	6	3.75	2.15	46.1
9-10E	7-8E	1	3.025	264.4	125.5
10-11E	"	2	3.085	9.5	17.7
8-9E	6-7E	1	3.335	435.9	187.7
9-10E	"	2	3.04	21.85	41.3
10-11E	"	3	3.105	1.15	5.3
7-8E	5-6E	1	2.91	227.55	112.3
8-9E	"	2	3.31	8.93	15.5
9-10E	"	3	3.13	0.73	3.3
10-11E	"	4	3.21	0.1	0.9
6-7E	4-5E	1	3.08	70.83	33
7-8E	"	2	2.985	15.63	30.1
8-9E	"	3	3.405	2.05	8.6
9-10E	"	4	3.11	0.2	1.8
10-11E	"	5	3.2	0.1	1.6
6-7E	3-4E	2	3.09	3.95	7.3
7-8E	"	3	2.99	5.5	26.4
8-9E	"	4	3.41	1	8.4

9-10E	"	5	3.105	0.2	3.2	
10-11E	"	6	3.2	0.1	2.5	
7-8E	2-3E	4	2.99	3.03	29.1	
8-9E	"	5	3.4	0.6	8.9	
9-10E	"	6	3.12	0.2	5.2	
7-8E	1-2E	5	2.99	2.38	40	
8-9E	"	6	3.4	0.5	11.8	
8-9E	10-11E	1	3.41	28.38	12	
7-8E	"	2	2.99	8.97	17.2	
6-7E	"	3	3.055	1.1	5.2	
9-10E	11-12E	1	3.13	32.2	14.8	
8-9E	"	2	3.4	1	1.7	
7-8E	"	3	3	1.1	5.3	
6-7E	"	4	3.09	0.2	1.9	
10-11E	12-13E	1	3.21	3.65	1.6	
9-10E	"	2	3.13	8.2	15.1	
8-9E	"	3	3.41	0.52	2.2	
7-8E	"	4	2.99	1.08	10.4	
6-7E	"	5	3.09	0.2	3.3	
10-11E	13-14E	2	3.21	0.9	1.6	
9-10E	"	3	3.12	3.43	15.8	
8-9E	"	4	3.41	0.38	3.2	
7-8E	"	5	3	0.9	15.1	
6-7E	"	6	3.09	0.2	5.2	
0-1W	1-2E	1	3.875	11.1	4.1	LINE 2
1-2W	"	2	4.665	13.7	16.9	
2-3W	"	3	4.445	1.3	4.2	
0-1E	2-3E	1	3.605	39	15.5	
0-1W	"	2	3.875	2.1	3.1	
1-2W	"	3	4.59	7.38	23.1	
2-3W	"	4	4.395	0.8	5.2	
1-2E	3-4E	1	3.34	29.68	12.8	
0-1E	"	2	3.605	1.7	2.7	
0-1W	"	3	3.895	0.8	3	
1-2W	"	4	4.605	3.43	21.4	
2-3W		5	4.395	0.4	4.6	
2-3E	4-5E	1	2.87	14.03	7	
1-2E	"	2	3.375	1.48	2.5	
0-1E	"	3	3.63	0.78	3.1	
0-1W	"	4	3.885	0.4	3	

1-2W	"	5	4.6	2.38	26
2-3W	"	6	4.395	0.3	5.5
2-3E	5-6E	2	2.895	0.45	0.9
1-2E	"	3	3.39	3.1	13.1
0-1E	"	4	3.61	0.75	6
0-1W	"	5	3.895	0.3	3.9
1-2W	"	6	4.59	1.63	28.6
2-3E	6-7E	3	2.895	0.53	2.6
1-2E	"	4	3.39	0.4	3.4
0-1E	"	5	3.67	0.35	4.8
0-1W	"	6	3.895	0.23	4.7
2-3E	7-8E	4	2.895	0.38	3.8
1-2E	"	5	3.4	0.2	3
0-1E	"	6	3.685	0.28	6.1
0-1E	1-2W	1	3.705	54.2	21
1-2E	"	2	3.5	10.8	17.7
2-3E	"	3	3	4.98	23.8
0-1W	2-3W	1	4.005	175.65	63
0-1E	"	2	3.785	3.65	5.5
1-2E	"	3	3.515	1.03	4.2
2-3E	"	4	3.02	0.56	5.3
1-2W	3-4W	1	4.66	152.1	46.9
0-1W	"	2	4.02	9.5	13.6
0-1E	"	3	3.81	1	3.8
1-2E	"	4	3.605	0.2	1.6
2-3E	"	5	3.115	0.2	3.2
2-3W	4-5W	1	4.425	35.55	11.5
1-2W	"	2	4.685	16.75	20.5
0-1W	"	3	4.005	2.13	7.6
0-1E	"	4	3.785	0.4	3
1-2E	"	5	3.555	0.2	2.8
2-3E	"	6	3.095	0.2	5.2
2-3W	5-6W	2	4.405	2.88	3.8
1-2W	"	3	4.66	7.68	23.7
0-1W	"	4	4.005	1.1	7.9
0-1E	"	5	3.785	0.23	3.1
1-2E	"	6	3.56	0.15	3.4
2-3W	6-7W	3	4.42	1.5	4.9
1-2W	"	4	4.65	4.95	30.6
0-1W	"	5	4.02	0.78	9.8
0-1E	"	6	3.79	0.2	4.2

2-3W	7-8W	4	4.405	1.03	6.7	
1-2W	"	5	4.67	3.73	40.2	
0-1W	"	6	4.035	0.68	13.6	
0-1E	1-2W	1	3.42	9	3.8	LINE 3
1-2E	"	2	3.53	5.7	9.3	
2-3E	"	3	3.755	2.43	9.3	
0-1W	2-3W	1	3.475	13.68	5.7	
0-1E	"	2	3.41	4.98	8.4	
1-2E	"	3	3.52	5.08	20.7	
2-3E	"	4	3.715	2.56	19.8	
1-2W	3-4W	1	3.535	30.38	12.3	
0-1W	"	2	3.485	3.45	5.7	
0-1E	"	3	3.415	1.88	7.9	
1-2E	"	4	3.5	2.2	18.1	
2-3E	"	5	3.69	1.3	17.7	
2-3W	4-5W	1	3.445	15.85	6.6	
1-2W	"	2	3.535	3.78	6.1	
0-1W	"	3	3.48	0.8	3.3	
0-1E	"	4	3.4	0.5	4.2	
1-2E	"	5	3.495	0.78	11.2	
2-3E	"	6	3.69	0.43	9.4	
2-3W	5-6W	2	3.505	4.2	6.9	
1-2W	"	3	3.59	1.5	6	
0-1W	"	4	3.52	0.4	3.3	
0-1E	"	5	3.48	0.3	4.3	
1-2E	"	6	3.57	0.4	9	
2-3W	6-7W	3	3.48	2.1	8.7	
1-2W	"	4	3.58	0.8	6.4	
0-1W	"	5	3.495	0.2	2.9	
0-1E	"	6	3.425	0.2	4.7	
2-3W	7-8W	4	3.455	1.1	9.1	
1-2W	"	5	3.585	0.5	7	
0-1W	"	6	3.505	0.2	4.6	
0-1W	1-2E	1	3.59	8.6	3.4	
1-2W	"	2	3.65	5.6	8.8	
2-3W	"	3	3.515	5.1	20.8	
0-1E	2-3E	1	3.53	7.9	3.2	
0-1W	"	2	3.595	2.2	3.5	
1-2W	"	3	3.675	2.23	8.7	
2-3W	"	4	3.55	2.45	19.8	

1-2E	3-4E	1	3.65	7.1	2.8	
0-1E	"	2	3.525	2.1	3.4	
0-1W	"	3	3.59	1.1	4.4	
1-2W	"	4	3.68	1.3	10.1	
2-3W	"	5	3.515	1.58	22.6	
2-3E	4-5E	1	3.79	6.05	2.3	
1-2E	"	2	3.615	2.72	4.3	
0-1E	"	3	3.515	1.06	4.3	
0-1W	"	4	3.58	0.6	4.8	
1-2W	"	5	3.645	0.7	9.7	
2-3W	"	6	3.51	0.9	20.6	
2-3E	5-6E	2	3.79	2	3	
1-2E	"	3	3.625	1.38	5.5	
0-1E	"	4	3.525	0.7	5.7	
0-1W	"	5	3.575	0.38	5.3	
1-2W	"	6	3.65	0.43	9.5	
2-3E	6-7E	3	3.795	1	3.8	
1-2E	"	4	3.62	0.95	7.5	
0-1E	"	5	3.51	0.4	5.7	
0-1W	"	6	3.585	0.2	4.5	
2-3E	7-8E	4	3.79	0.64	4.9	
1-2E	"	5	3.62	0.68	9.4	
0-1E	"	6	3.515	0.2	4.6	
0-1W	1-2E	1	4.19	149.65	51.3	LINE 4
1-2W	"	2	4.405	2.7	3.5	
2-3W	"	3	4.37	1.1	3.6	
0-1E	2-3E	1	4.035	11.9	4.2	
0-1W	"	2	4.145	1.8	2.5	
1-2W	"	3	4.355	1	3.3	
2-3W	"	4	4.32	0.6	4	
1-2E	3-4E	1	3.09	8.45	3.9	
0-1E	"	2	3.985	1.63	2.4	
0-1W	"	3	4.105	0.9	3.1	
1-2W	"	4	4.325	0.7	4.6	
2-3W	"	5	4.265	0.48	5.7	
2-3E	4-5E	1	3.105	6.63	3.1	
1-2E	"	2	3.075	1.68	3.1	
0-1E	"	3	3.99	1.46	5.3	
0-1W	"	4	4.09	1.06	7.4	
1-2W	"	5	4.305	0.88	10.3	
2-3W	"	6	4.22	0.68	13	

2-3E	5-6E	2	3.09	0.88	1.6
1-2E	"	3	3.01	0.82	3.9
0-1E	"	4	3.925	1	7.3
0-1W	"	5	4.05	0.78	9.7
1-2W	"	6	4.295	0.7	13.1
2-3E	6-7E	3	3.08	2.2	10.3
1-2E	"	4	3.015	0.7	6.7
0-1E	"	5	3.915	0.58	7.4
0-1W	"	6	4.06	0.43	8.5
2-3E	7-8E	4	3.085	0.8	7.4
1-2E	"	5	3.015	0.4	6.7
0-1E	"	6	3.91	0.5	10.3
0-1E	1-2W	1	3.955	76.15	27.7
1-2E	"	2	3.025	1.9	3.6
2-3W	"	3	3.095	0.7	3.2
0-1W	2-3W	1	4.075	12.4	4.4
0-1E	"	2	3.915	2.15	3.2
1-2E	"	3	3.02	0.78	3.7
2-3E	"	4	3.09	0.5	4.6
1-2W	3-4W	1	4.3	15.33	5.1
0-1W	"	2	4.065	2.2	3.1
0-1E	"	3	3.96	0.9	3.3
1-2E	"	4	3.035	0.43	4.1
2-3E	"	5	3.09	0.3	4.9
2-3W	4-5W	1	4.205	52.7	18
1-2W	"	2	4.27	2.1	2.8
0-1W	"	3	4.02	0.9	3.2
0-1E	"	4	3.945	0.5	3.6
1-2E	"	5	3.025	0.2	3.3
2-3E	"	6	3.085	0.2	5.2
2-3W	5-6W	2	4.2	3.9	5.3
1-2W	"	3	4.27	0.98	3.3
0-1W	"	4	4.015	0.58	4.1
0-1E	"	5	3.93	0.4	5.1
1-2E	"	6	3	0.2	5.4
2-3W	6-7W	3	4.23	0.8	2.7
1-2W	"	4	4.305	0.45	3
0-1W	"	5	4.05	0.4	5
0-1E	"	6	3.925	0.2	4.1
2-3W	7-8W	4	4.205	0.55	3.8

1-2W	"	5	4.29	0.35	4.1	
0-1W	"	6	4.03	0.25	5	
0-1W	1-2E	1	4.305	49.17	16.4	LINE 5
1-2W	"	2	3.715	2	3.1	
2-3W	"	3	3.285	0.5	2.2	
0-1E	2-3E	1	3.585	9.7	3.9	
0-1W	"	2	4.295	1.7	2.3	
1-2W	"	3	3.705	0.7	2.7	
2-3W	"	4	3.23	0.37	3.3	
1-2E	3-4E	1	3.315	13.4	5.8	
0-1E	"	2	3.555	1.48	2.4	
0-1W	"	3	4.285	0.7	2.3	
1-2W	"	4	3.69	0.53	4.1	
2-3W	"	5	3.22	0.3	4.7	
2-3E	4-5E	1	2.82	6.3	3.2	
1-2E	"	2	3.345	1.25	2.1	
0-1E	"	3	3.59	0.78	3.1	
0-1W	"	4	4.285	0.4	2.7	
1-2W	"	5	3.695	0.38	5.2	
2-3W	"	6	3.2	0.2	5	
2-3E	5-6E	2	2.82	0.45	0.9	
1-2E	"	3	3.34	0.55	2.4	
0-1E	"	4	3.6	0.48	3.8	
0-1W		5	4.25	0.33	3.9	
1-2W	"	6	3.68	0.3	6.6	
2-3E	6-7E	3	2.85	2.07	10.4	
1-2E	"	4	3.34	0.8	6.9	
0-1E	"	5	3.59	0.4	5.6	
0-1W	"	6	4.22	0.3	5.7	
2-3E	7-8E	4	2.865	0.58	5.8	
1-2E	"	5	3.38	0.33	4.9	
0-1E	"	6	3.59	0.3	6.7	
0-1E	1-2W	1	3.995	75.63	27.2	
1-2E	"	2	3.77	1.87	2.8	
2-3E	"	3	3.105	0.6	2.8	
0-1W	2-3W	1	4.6	51.18	16	
0-1E	"	2	3.98	1.83	2.6	
1-2E	"	3	3.7	0.5	1.9	
2-3E	"	4	3.08	0.35	3.3	
1-2W	3-4W	1	3.92	68.08	24.9	

0-1W	"	2	4.505	2.02	2.6	
0-1E	"	3	3.88	0.68	2.5	
1-2E	"	4	3.65	0.33	2.6	
2-3E	"	5	3.01	0.22	3.7	
2-3W	4-5W	1	3.36	48.58	20.8	
1-2W	"	2	3.885	2.14	3.2	
0-1W	"	3	4.46	0.8	2.6	
0-1E	"	4	3.86	0.4	3	
1-2E	"	5	3.62	0.23	3.2	
2-3E	"	6	3	0.2	5.4	
2-3W	5-6W	2	3.34	2.08	3.6	
1-2W	"	3	3.88	0.73	2.7	
0-1W	"	4	4.42	0.4	2.6	
0-1E	"	5	3.83	0.3	3.9	
1-2E	"	6	3.6	0.2	4.5	
2-3W	6-7W	3	3.31	0.63	2.7	
1-2W	"	4	3.86	0.38	2.8	
0-1W	"	5	4.4	0.25	2.9	
0-1E	"	6	3.83	0.2	4.2	
2-3W	7-8W	4	3.3	0.4	3.5	
1-2W	"	5	3.82	0.3	3.9	
0-1W	"	6	4.4	0.25	4.6	
0-1S	1-2N	1	3.7	46.1	17.9	LINE 6
1-2S	"	2	4.01	6.65	9.5	
2-3S	"	3	3.79	1.7	6.4	
0-1N	2-3N	1	3.695	61.98	24.1	
0-1S	"	2	3.67	6.7	10.5	
1-2S	"	3	3.99	1.65	5.9	
2-3S	"	4	3.79	0.6	4.5	
1-2N	3-4N	1	3.7	28.48	11.1	
0-1N	"	2	3.69	5	7.8	
0-1S	"	3	3.62	1	4	
1-2S	"	4	3.95	0.4	2.9	
2-3S	"	5	3.73	0.3	4	
2-3N	4-5N	1	3.38	49.23	20.9	
1-2N	"	2	3.67	4.9	7.7	
0-1N	"	3	3.67	1.58	6.2	
0-1S	"	4	3.625	0.48	3.8	
1-2S	"	5	3.9	0.3	3.9	
2-3S	"	6	3.7	0.2	4.3	
2-3N	5-6N	2	3.38	7.87	13.4	

1-2N	"	3	3.68	1.15	4.5
0-1N	"	4	3.66	0.53	4.2
0-1S	"	5	3.62	0.2	2.8
1-2S	"	6	3.91	0.2	4.1
2-3N	6-7N	3	3.39	1.7	7.2
1-2N	"	4	3.7	0.43	3.3
0-1N	"	5	3.645	0.3	4.1
0-1S	"	6	3.61	0.2	4.5
2-3N	7-8N	4	3.37	0.53	4.5
1-2N	"	5	3.67	0.2	2.7
0-1N	"	6	3.63	0.2	4.4
0-1N	1-2S	1	3.69	47.2	18.4
1-2N	"	2	3.7	6.03	9.4
2-3N	"	3	3.4	1.35	5.7
0-1S	2-3S	1	3.7	70.23	27.3
0-1N	"	2	3.7	8.47	13.2
1-2N	"	3	3.725	1.6	6.2
2-3N	"	4	3.41	0.58	4.9
1-2S	3-4S	1	3.95	96.5	35.1
0-1S	"	2	3.66	11.8	18.5
0-1N	"	3	3.69	2.18	8.5
1-2N	"	4	3.7	0.5	3.9
2-3N	"	5	3.4	0.2	3
2-3S	4-5S	1	3.7	84.1	32.6
1-2S	"	2	3.95	15.28	22.2
0-1S	"	3	3.67	3.2	12.5
0-1N	"	4	3.685	0.8	6.2
1-2N	"	5	3.695	0.3	4.1
2-3N	"	6	3.41	0.2	4.7
2-3S	5-6S	2	3.69	19.8	30.8
1-2S	"	3	3.95	4.9	17.8
0-1S	"	4	3.67	1.2	9.4
0-1N	"	5	3.7	0.38	5.2
1-2N	"	6	3.71	0.2	4.3
2-3S	6-7S	3	3.7	4.2	16.3
1-2S	"	4	3.95	1.2	8.7
0-1S	"	5	3.67	0.43	5.9
0-1N	"	6	3.7	0.2	4.3
2-3S	7-8S	4	3.7	1	7.8
1-2S	"	5	3.96	0.4	5.1
0-1S	"	6	3.67	0.2	4.4